Supplementary Information (SI) for Journal of Materials Chemistry C.

Supporting Information

Self-Assembled Monolayer Engineering Facilitates the Sensitivity and Response Speed of High-Performance Perovskite Photodetectors

Hailong Hu[1], Yongpeng Huang[1], Wanhai Wang[2], Yikai Yun[1], Shaoqun Li[1], Lihua Lu[1], Sijie Jiang[1], Xuanwei Chen[1], Weihua Tang[2*], Mengyu Chen[1,3*], Cheng Li[1,3*]

[1]School of Electronic Science and Engineering, Xiamen University, Xiamen 361005, P. R. China

[2]College of Materials, College of Chemistry and Chemical Engineering, Innovation Laboratory for Sciences and Technologies of Energy Materials of Fujian Province (IKKEM), Xiamen University, Xiamen 361005, P. R. China

[3]Future Display Institute of Xiamen, Xiamen 361005, P. R. China

*Correspondence to: mychen@xmu.edu.cn; chengli@xmu.edu.cn; whtang@xmu.edu.cn;

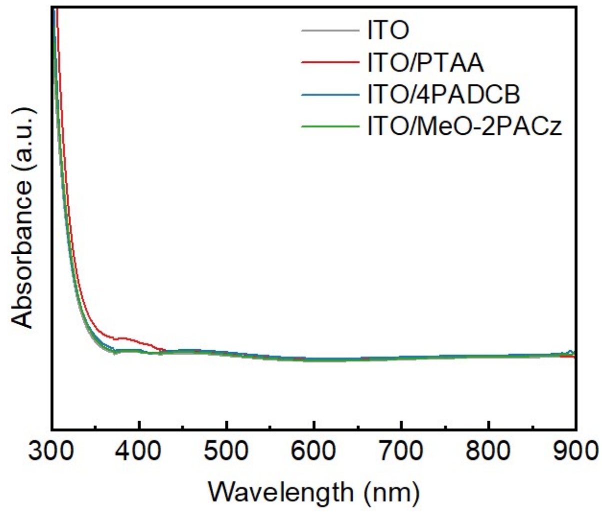

Figure S1. UV–vis transmission spectra of bare ITO, PTAA-coated ITO, MeO-2PACz-coated ITO, and 4PADCB-coated ITO substrates.

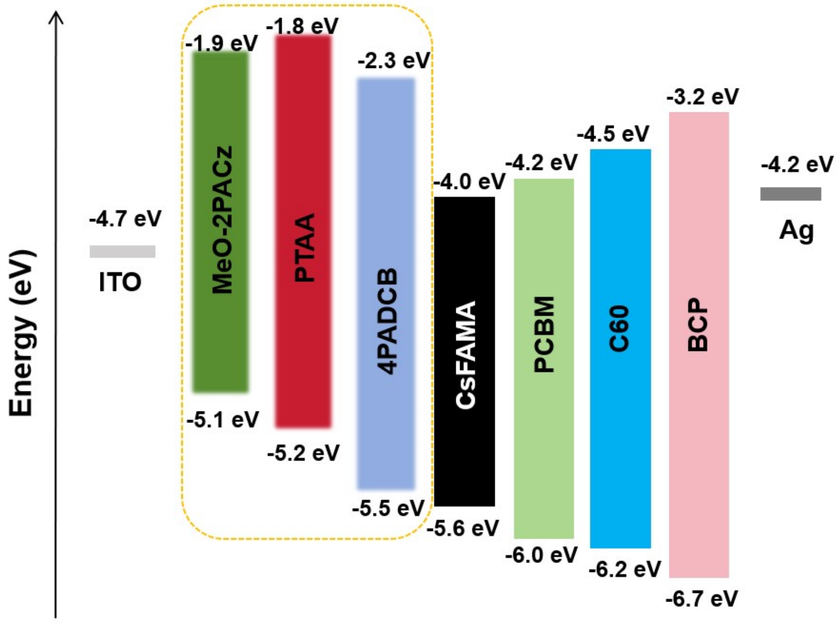

Figure S2. Energy-level diagram of the perovskite photodetectors based on different HTLs (4PADCB, MeO-2PACz, and PTAA).

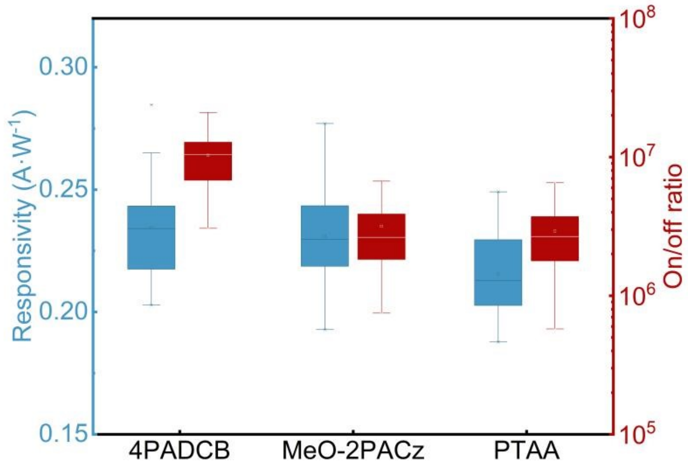

Figure S3. The statistical distributions of responsivity, and on/off ratio for perovskite photodetectors (PPDs) with different hole transport layers (HTLs), tested at AM 1.5G solar spectrum condition.

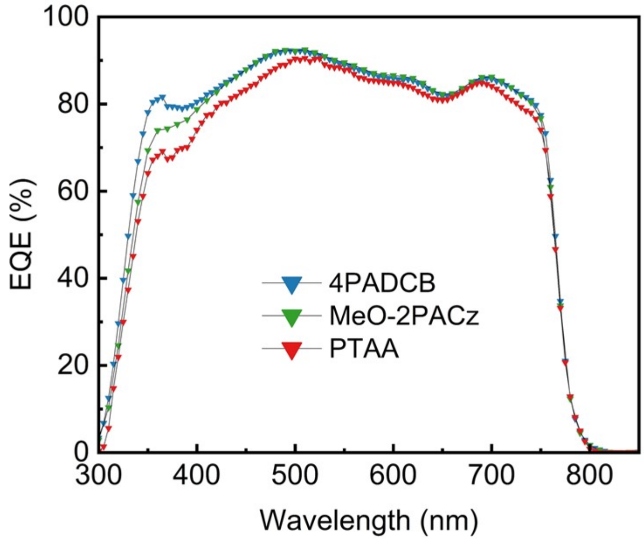

Figure S4. The external quantum efficiency (EQE) of PPDs with different HTLs.

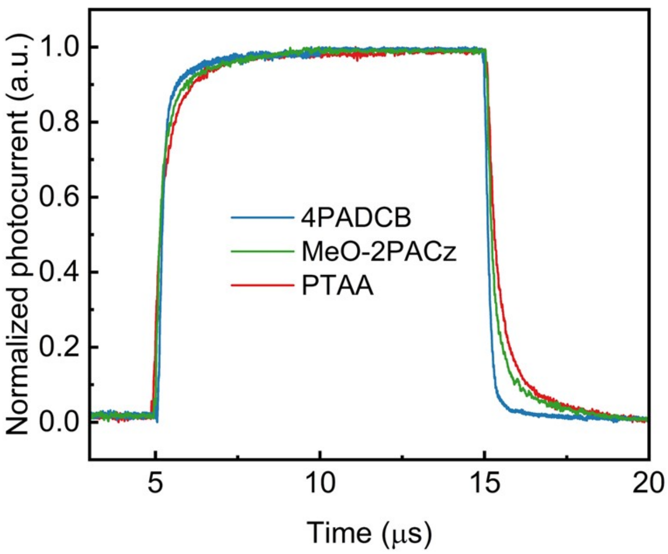

Figure S5. The transient response of PPDs based on different HTLs.

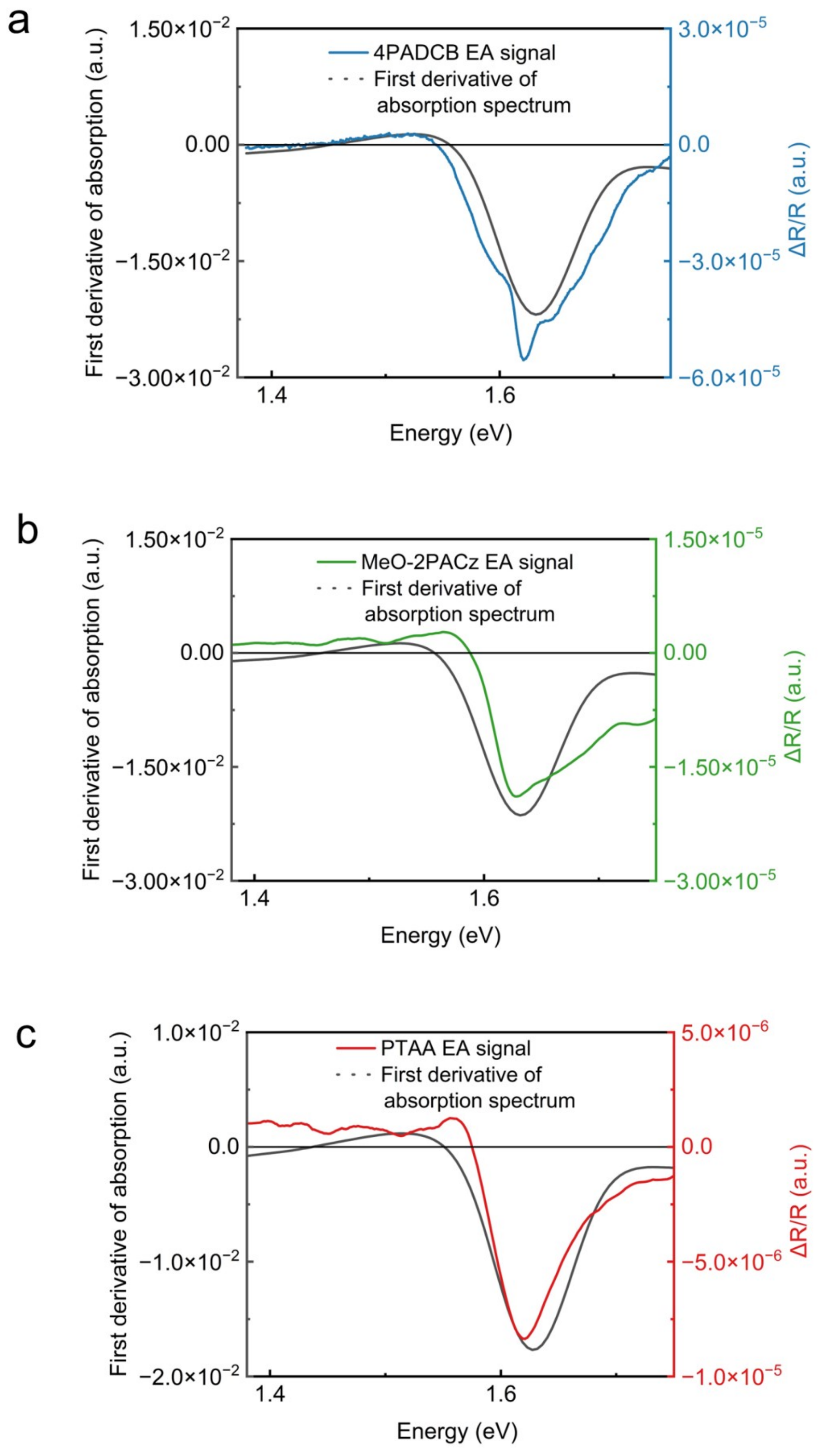

Figure S6. EA spectrum and the first derivative of the corresponding light absorption spectrum of the perovskite film deposited on (a)4PADCB, (b)MeO-2PACz and (c) PTAA.

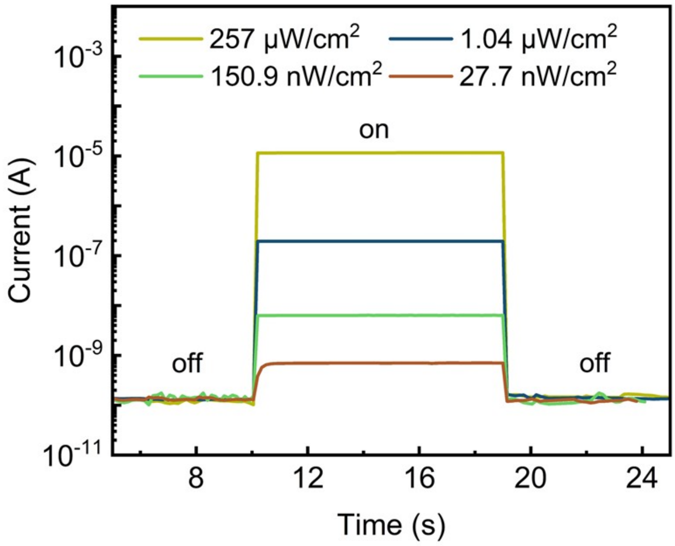

Figure S7. The I-T curve under different weak light illuminations at 520 nm.

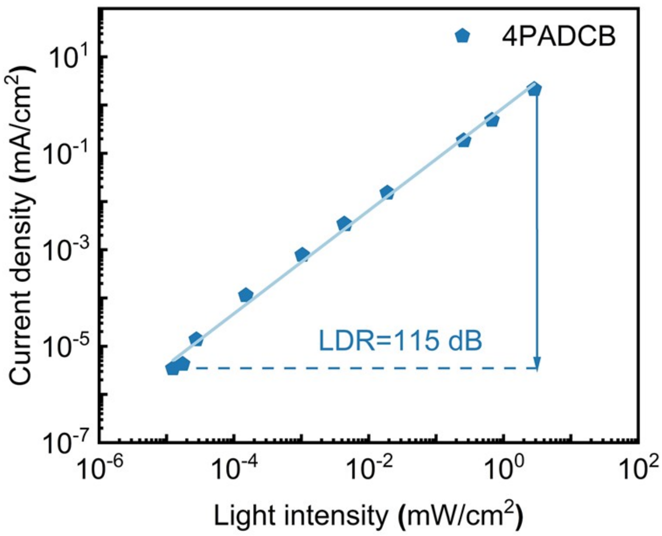

Figure S8. Linear dynamic range of 4PADCB-based perovskite photodetectors measured under zero bias voltage and illumination with a 520 nm light source at varying light intensities.

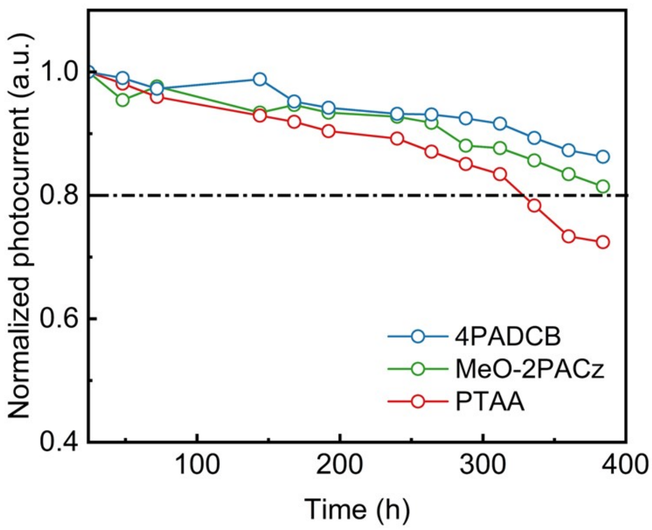

Figure S9. The storage stability of unsealed devices with different HTLs under ambient air conditions with a relative humidity of 25±5%.

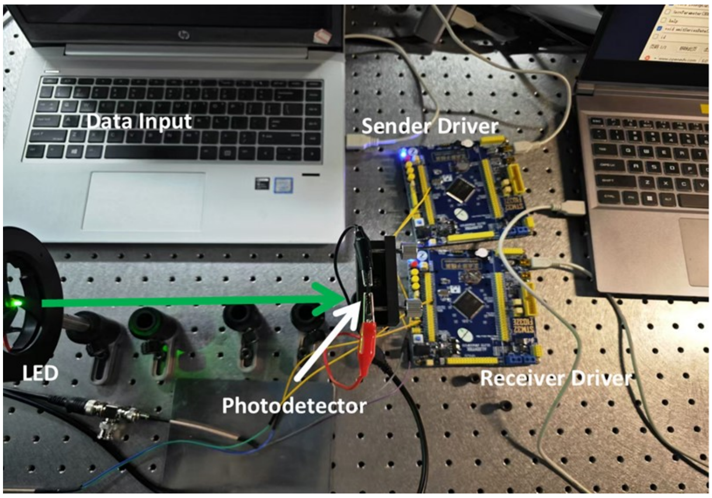

Figure S10. Photograph of the visible light communication application based on perovskite photodetectors.

Table S1. Results of the full width at half maximum (FWHM) from the X-ray diffraction (XRD) pattern.

HTL	(101)	(211)	(024)	(202)	(131)
4PADCB	0.23	0.19	0.21	0.19	0.22
MeO-2PACz	0.24	0.20	0.20	0.20	0.22
PTAA	0.28	0.22	0.22	0.20	0.25

Table S2. Summary of fitted lifetimes for perovskite films from TRPL spectra.

HTL	A_1	τ_1 (ns)	A_2	τ_2 (ns)	τ_{ave} (ns)
4PADCB	14.49	26.79	0.26	3665.53	2605.77
MeO-2PACz	2.21	69.89	0.27	2485.31	2033.31
PTAA	718.71	14.24	0.39	496.44	23.33

Table S3. Summary of fitted transient photocurrent (TPC) decay curve for devices with different HTLs, where the 4PADCB-based device follows a single-exponential fit.

HTL	A_1	τ_1 (ns)	A_2	τ_2 (μs)
(single-exponential fit)				
4PADCB	1.03	155	\	\
(double-exponential fit)				
4PADCB	1.04	149	0.03	5.03
MeO-2PACz	0.89	251	0.14	2.91
PTAA	0.89	353	0.18	3.39

Table S4. Summary of R_s, R_{rec}, C, and τ_{RC} extracted from EIS measurements under dark conditions for devices with different HTLs.

HTL	R_s (Ω)	R_{rec} (kΩ)	C (nF)	τ_{RC} (s)
4PADCB	10.2	9.43	7.44	7.58×10^{-8}
MeO-2PACz	42.1	7.85	3.21	1.34×10^{-7}
PTAA	30.9	4.25	9.37	2.87×10^{-7}

Supplementary Note 1. Calculation of the RC Time Constant (τ_{RC})

The RC time constant (τ_{RC}) of the perovskite photodetectors is determined by the device's series resistance (R_s), recombination resistance (R_{rec}), and capacitance (C), according to the following relation[1]:

$$\tau_{RC} = \frac{C}{\frac{1}{R_S} + \frac{1}{R_{rec}}} \tag{1}$$

Given that the fitted recombination resistance (R_{rec}) is much larger than the series resistance (R_s) (R_{rec} >> R_s) for all devices, the contribution of R_{rec} to τ_{RC} can be neglected. Therefore, the expression simplifies to:

$$\tau_{RC} \approx R_S \cdot C \tag{2}$$

Based on the EIS fitting parameters summarized in Table S4, the 4PADCB-based device exhibits the smallest R_s and C values among the three devices. This leads to a reduced τ_{RC} of 7.58×10^{-8} s, which significantly enhances the device's modulation bandwidth.

Table S5. Comparison of photodetection performances of our fabricated perovskite photodetector devices with counterparts in literatures.

Device Structure	R ($A \cdot W^{-1}$)	D^* (Jones)	Area (cm^2)	rise/fall time	Ref.
ITO/NiO_x/$CH_3NH_3PbI_3$/PCBM/BCP/Ag	1.06	7.28×10^{12}	2.5×10^{-5}	5 μs/18 μs	2
ITO/blend SAMs/CsFAMA/C60/BCP/Ag	0.41	6.4×10^{11}	-	-	3
ITO/PTAA/Perovskite/C60/BCP/Cu	0.45	1.45×10^{12}	0.1	0.9 μs/1.3 μs	4
ITO/NiO_x/Perovskite/PCBM/Bphen/Ag	0.35	1.46×10^{12}	0.0025	1.03 μs/3.02 μs	5
ITO/MeO-2PACz/Perovskite/PCBM/BCP/Ag	0.44	8.7×10^{12}	-	580 ns/180 ns	6
ITO/PEDOT:PSS/Perovskite/PCBM/Ag	-	2.8×10^{13}	0.04	16.3 μs/23.9 μs	7
ITO/4PADCB/CsFAMA/PCBM/C60/BCP/Ag	0.48	1.56×10^{13}	0.06	546 ns/334 ns	this work

References

1 S. Li, Y. Yun, W. Wei, J. Du, S. Jiang, Y. Tian, H. Luo, K. Huang, C. Li, M. Chen and R. Zhang, *ACS Photonics*, 2024, **11**, 4716–4724.

2 D.-D. Zhang, H.-X. Wei and L.-Q. Zhu, *Organic Electronics*, 2023, **114**, 106726.

3 E. Angela, D. Nodari, F. Furlan, J. Panidi, M. A. McLachlan and N. Gasparini, *ACS Appl. Mater. Interfaces*, 2024, **16**, 33838–33845.

4 X. Feng, M. Tan, M. Li, H. Wei and B. Yang, *Nano Lett.*, 2021, **21**, 1500–1507.

5 Z.-Y. Yin, Y. Chen, Y.-Y. Zhang, Y. Yuan, Q. Yang, Y.-N. Zhong, X. Gao, J. Xiao, Z.-K. Wang, J.-L. Xu and S.-D. Wang, *Advanced Functional Materials*, 2023, **33**, 2302199.

6 F. Furlan, D. Nodari, E. Palladino, E. Angela, L. Mohan, J. Briscoe, M. J. Fuchter, T. J. Macdonald, G. Grancini, M. A. McLachlan and N. Gasparini, *Advanced Optical Materials*, 2022, **10**, 2201816.

7 Y. Liu, Z. Liu, Z. Zhang, J. Huang, X. Li, H. Yu, Y. Shen, M. Wang and G. Tu, *J. Mater. Chem. C*, 2024, **12**, 9944–9949.